NASA Technical Memorandum 85890 USAAVSCOM Technical Memorandum 84-A-2

A Mathematical Model of the UH-60 Helicopter

Kathryn B. Hilbert, Aeromechanics Laboratory,
U.S. Army Research and Technology Laboratories-AVSCOM
Ames Research Center, Moffett Field, California

NASA
National Aeronautics and Space Administration

Ames Research Center
Moffett Field, California 94035

United States Army
Aviation Systems
Command
St. Louis, Missouri 63120

SYMBOLS

a blade lift-curve slope, per rad

a_o blade coning angle measured from hub plane in the hub-wind axes system, rad

a_1 longitudinal first-harmonic flapping coefficient measured from the hub plane in the wind-hub axes system, rad

a_y lateral acceleration, m/sec^2 (ft/sec^2)

b_1 lateral first-harmonic flapping coefficient measured from hub plane in the wind-hub axes system, rad

C_T rotor thrust coefficient, $T/\rho(\pi R^2)(\Omega R)^2$

D Drag force, N (lb)

H rotor force normal to shaft, positive downwind, N (lb)

i_{HS} incidence of horizontal stabilator, positive for leading edge up, rad

K tail rotor cant angle, rad

K_1 pitch-flap coupling ratio, $\triangleq \tan \delta_3$

ℓ fuselage rolling moment, N-m (ft-lb)

L fuselage lift, N (lb)

$\left.\begin{matrix} L \\ M \\ N \end{matrix}\right\}$ rolling moment, pitching moment, and yawing moment, respectively, N-m (ft-lb)

$\left.\begin{matrix} p \\ q \\ r \end{matrix}\right\}$ roll, pitch, and yaw rates in the body-c.g. axes system, rad/sec

q dynamic pressure, $\frac{1}{2}\rho V^2$, N/m^2 (lb/ft^2)

Q torque, N-m (ft-lb)

R rotor radius, m (ft)

STA longitudinal location in the fuselage axes system, m (ft)

T thrust, N (lb)

$\left.\begin{array}{l} u \\ v \\ w \end{array}\right\}$ longitudinal, lateral, and vertical velocities in the body-c.g. system of axes, m/sec (ft/sec)

$v_{i_{TR}}$ tail rotor induced velocity at rotor disk, m/sec (ft/sec)

WL vertical location in the fuselage axes system, m (ft)

$\left.\begin{array}{l} X \\ Y \\ Z \end{array}\right\}$ longitudinal, lateral, and vertical forces in the body-c.g. axes system, N (lb)

α Stabilizing surface angle of attack, rad

β_w rotor sideslip angle, rad

γ blade Lock number, $\rho acR^4/I_\beta$

δ equivalent rotor blade profile drag coefficient

δ_a lateral cyclic stick movement, positive to right, cm (in.)

δ_c collective control input, positive up, cm (in.)

δ_e longitudinal cyclic stick movement, positive aft, cm (in.)

δ_p pedal movement, positive right, cm (in.)

Δ increment in

θ Euler pitch angle, rad

θ_o blade root collective pitch, rad

θ_t total blade twist (root minus tip incidence), rad

λ inflow ratio, $\triangleq \frac{w_H}{\Omega} - \frac{C_T}{2(\mu^2 + \lambda^2)^{1/2}}$

μ rotor advance ratio, $\frac{\sqrt{u_H^2 + v_H^2}}{\Omega R}$

ρ air density, kg/m^3 (slugs/ft^3)

σ rotor solidity ratio, blade area/disk area

ϕ Euler roll angle, rad

ψ Euler yaw angle, rad

Ω rotor angular velocity, rad/sec

Subscripts:

B	body-c.g. axes system relative to air mass
C	cant axes system
CW	cant-wind axes system
c.g.	center of gravity
f	fuselage
H	hub-body axes system, hub location
HS	horizontal stabilator
i	induced
p	pilot input
TR	tail rotor
W	hub-wind system of axes

SUMMARY

This report documents the revisions made to a mathematical model of a single main rotor helicopter. These revisions were necessary to model the UH-60 helicopter accurately. The major modifications to the model include fuselage aerodynamic force and moment equations that are specific to the UH-60, a canted tail rotor, a horizontal stabilator with variable incidence, and a pitch bias actuator (PBA). In addition, the model requires a full set of parameters which describe the helicopter configuration and its physical characteristics.

INTRODUCTION

A ten-degree-of-freedom, nonlinear mathematical model that is suitable for real-time piloted simulation of single rotor helicopters is described in reference 1. This simulation model includes the rigid body equations of motion and an aerodynamic model that provide the aerodynamic force and moment characteristics of the aircraft, a generalized stability and control augmentation system, and a simplified engine/governor model.

Revisions to the model were made with the following objectives:

1. Improvement of the fidelity of the UH-60 fuselage aerodynamic model over a wide range of angles of attack and sideslip angles.

2. Modification of the tail rotor aerodynamic model to include the option of canting the tail rotor and modeling its associated aerodynamic effects.

3. Incorporation in the model of the control system for the UH-60 horizontal stabilator with variable incidence and the resultant aerodynamic effects.

4. Incorporation of the UH-60's pitch bias actuator as part of the stability and control augmentation system.

This report describes the four major modifications to the model; the fuselage aerodynamic force and moment equations that are specific to the UH-60, a canted tail rotor, the UH-60 horizontal stabilator with variable incidence, and the UH-60 pitch bias actuator. In addition, a section describing the physical characteristics of the UH-60 and the parameters required by the model is also included.

REVISIONS TO THE FUSELAGE AERODYNAMICS

The UH-60's fuselage aerodynamics were modeled using extensive wind-tunnel test data presented in reference 2. The fuselage force and moment equations were derived from these test data using a regression algorithm (ref. 3). This algorithm basically fits a curve to input data as a nonlinear function of several aerodynamic variables that are specified by the user (ψ, α, sin ψ, ψ^2, . . .). These equations replace the fuselage force and moment equations given in reference 1 since they are specific to the UH-60 helicopter.

The equations derived depend on the conventional definition of the angles of attack and sideslip used in the wind tunnel. These angles are not Euler angles. The angle of attack is the geometric angle subtended by the model relative to tunnel axis at zero yaw angle. It is measured relative to the tunnel floor and does not change with yaw angle.

$$\alpha_f \triangleq \theta_w \triangleq \tan^{-1} \frac{w_f}{|u_B|}$$

where

$$w_f \triangleq w_B + q_B(STA_f - STA_{c.g.}) - w_{i_f}$$

The sideslip angle is the yaw table angle in the horizontal plane of the tunnel, irrespective of the angle of attack.

$$\beta_{w_f} \triangleq -\psi_w \triangleq \tan^{-1} \frac{v_f}{\sqrt{u_B^2 + w_f^2}}$$

where

$$v_f \triangleq v_B - r_B(STA_f - STA_{c.g.})$$

The longitudinal forces and moments are dependent on both the angle of attack and on the sideslip angle. The lateral forces and moments are dependent only on the sideslip angle.

Forces:

Drag: $$\frac{D}{q} = 90.0555 \sin^2 \alpha_f - 41.5604 \cos \alpha_f + 2.94684 \cos 4\psi_w - 103.141 \cos 2\psi_w - 0.535350\times10^{-6} \psi_w^4 + 160.2049$$

Lift: $$\frac{L}{q} = 29.3616 \sin \alpha_f + 43.4680 \sin 2\alpha_f - 81.8924 \sin^2 \alpha_f - 84.1469 \cos \alpha_f - 0.821406\times10^{-1} \psi_w + 3.00102 \sin 4\psi_w + 0.0323477 \psi_w^2 + 85.3496$$

Sideforce: $$\frac{Y}{q} = 35.3999 \sin \psi_w + 71.8019 \sin 2\psi_w - 8.04823 \sin 4\psi_w - 0.980257\times10^{-12}$$

Moments:

Pitching: $$\frac{M}{q} = 2.37925 \alpha_f + 728.026 \sin 2\alpha_f + 426.760 \sin^2 \alpha_f + 348.072 \cos \alpha_f - 510.581 \cos^3 \psi_w + 56.111$$

Rolling: $$\frac{\ell}{q} = 614.797 \sin \psi_w + \frac{\psi_w}{|\psi_w|} (-47.7213 \cos 4\psi_w - 290.504 \cos^3 \psi_w + 735.507 \cos^4 \psi_w - 669.266) \qquad 25^\circ < |\psi_w| \leq 90^\circ$$

$$\frac{\ell}{q} = \frac{\psi_w}{|\psi_w|}(455.707 \cos^4 \psi_w - 428.639) \qquad 10° < |\psi_w| \leq 25°$$

$$\frac{\ell}{q} = 0.0 \qquad -10° \leq \psi_w \leq 10°$$

Yawing: $$\frac{N}{q} = 220.0 \sin 2\psi_w + \frac{\psi_w}{|\psi_w|}(671.0 \cos^4 \psi_w - 429.0) \qquad 20° < |\psi_w| \leq 90°$$

$$\frac{N}{q} = -278.133 \sin 2\psi_w + 422.644 \sin 4\psi_w - 1.83172 \qquad -20° \leq \psi_w \leq 20°$$

Plots of fuselage drag, lift and pitching moment vs the angle of attack are shown in figures 1, 2, and 3. Plots of incremental drag, lift, and pitching moment vs sideslip ($\beta_{w_f} = -\psi_w$) are shown in figures 4, 5, and 6. Figures 7, 8, and 9 show fuselage sideforce, rolling and yawing moments vs sideslip. For all these plots, the wind-tunnel data are shown as well as the data generated from the equations derived using the regression algorithm.

CANTED TAIL ROTOR

The UH-60 helicopter was designed with a canted tail rotor mounted on the right side of the vertical fin. In order to find the aerodynamic force and moment contributions from the canted tail rotor it was necessary to introduce two additional axes systems: the cant axis system (subscript C), and the cant-wind axis system (subscript CW). Once these axes systems and the transformations between them have been defined, the development of the tail rotor flapping, force, and moment equations parallels the development done in reference 1 for a noncanted tail rotor (sketch A).

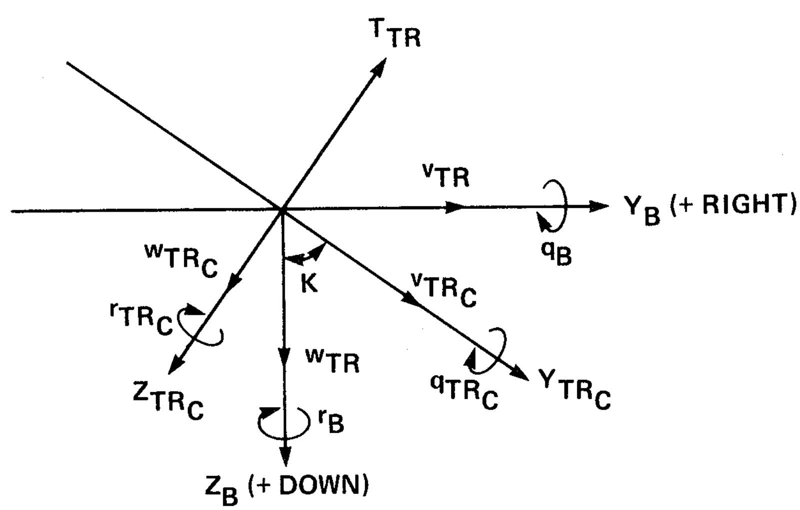

Sketch A

The velocities at the rotor hub in the cant axis system are:

$$u_{TR_C} = u_{TR}$$

$$v_{TR_C} = w_{TR} \cos K + v_{TR} \sin K$$

$$w_{TR_C} = -v_{TR} \cos K + w_{TR} \sin K$$

where K = tail rotor cant angle. So when $K = 0°$, the cant axis system coincides with the axis system codirectional with the body-c.g. system.

$$v_{TR_C} = w_{TR} \,, \qquad w_{TR_C} = -v_{TR}$$

The advance ratio for the tail rotor in the cant axis system is:

$$\mu_{TR_C} = \frac{\sqrt{u_{TR_C}^2 + v_{TR_C}^2}}{R_{TR}\Omega_{TR}}$$

The angles of attack and sideslip for the tail rotor in the cant axis system are defined as (sketch B):

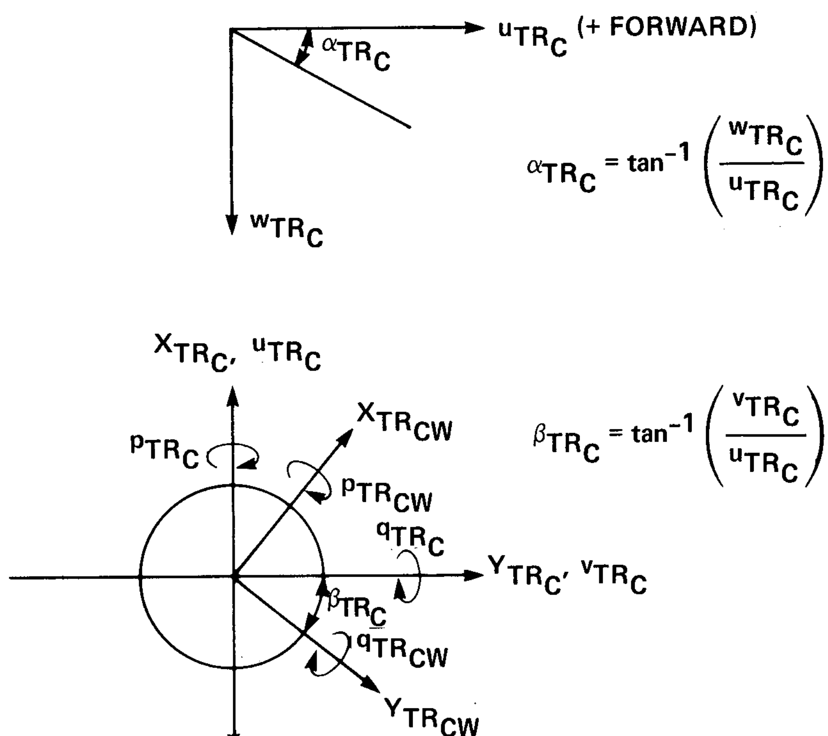

Sketch B

The angular velocities in the cant axis system are:

$$p_{TR_C} = p_B$$

$$q_{TR_C} = r_B \cos K + q_B \sin K$$

$$r_{TR_C} = -q_B \cos K + r_B \sin K$$

The roll and pitch rates in the cant-wind axis system are:

$$p_{TR_{CW}} = q_{TR_C} \sin \beta_{TR_C} + p_{TR_C} \cos \beta_{TR_C}$$

$$q_{TR_{CW}} = -p_{TR_C} \sin \beta_{TR_C} + q_{TR_C} \cos \beta_{TR_C}$$

The flapping coefficients are:

$$a_{1_{TR_C}} = \frac{1}{\Delta_{TR_C}} \left[K_{1_{TR}} \left(1 + \frac{3}{2} \mu_{TR_C}^2\right) f_{1_{TR_C}} - \left(1 + \frac{\mu_{TR_C}^2}{2}\right) f_{2_{TR_C}} \right]$$

$$b_{1_{TR_C}} = \frac{1}{\Delta_{TR_C}} \left[\left(1 - \frac{\mu_{TR_C}^2}{2}\right) f_{1_{TR_C}} + K_{1_{TR}} \left(1 + \frac{\mu_{TR_C}^2}{2}\right) f_{2_{TR_C}} \right]$$

where:

$$\Delta_{TR_C} = 1 - \frac{\mu_{TR_C}^4}{4} + K_{1_{TR}}^2 \left(1 + \frac{\mu_{TR_C}^2}{2}\right) \left(1 + \frac{3}{2} \mu_{TR_C}^2\right)$$

$$f_{1_{TR_C}} = \frac{4}{3} \mu_{TR_C} a_{o_{TR}} - \frac{16}{\gamma_{TR} \Omega_{TR}} p_{TR_{CW}} - \frac{q_{TR_{CW}}}{\Omega_{TR}}$$

$$f_{2_{TR_C}} = \frac{8}{3} K_{1_{TR}} \mu_{TR_C} a_{o_{TR}} + \frac{16 q_{TR_{CW}}}{\gamma_{TR} \Omega_{TR}} - \mu_{TR_C} \left(\frac{8}{3} \theta_{o_{TR}} + 2\theta_{t_{TR}} + 2\lambda_{TR}\right) - \frac{p_{TR_{CW}}}{\Omega_{TR}}$$

The forces on the tail rotor in the cant-wind axis system ($T_{TR_{CW}}$, $H_{TR_{CW}}$, $Y_{TR_{CW}}$, $Q_{TR_{CW}}$) are the same as the equations given in reference 1 with μ_{TR}, p_{TR}, q_{TR}, $a_{1_{TR}}$, $b_{1_{TR}}$, and δ_{TR} replaced by μ_{TR_C}, $p_{TR_{CW}}$, $q_{TR_{CW}}$, $a_{1_{TR_C}}$, $b_{1_{TR_C}}$, and δ_{TR_C}, respectively, where the rotor blade profile drag coefficient is:

$$\delta_{TR_C} = 0.009 + 0.3 \left(\frac{6 C_{T_{TR_{CW}}}}{\sigma_{TR} a_{TR}} \right)^2$$

and the inflow ratio is:

$$\lambda_{TR} = \frac{w_{TR_C}}{\Omega_{TR} R_{TR}} - \frac{C_{T_{TR_{CW}}}}{2\sqrt{\mu_{TR_C}^2 + \lambda_{TR}^2}}$$

The induced velocity at the tail rotor is:

$$v_{i_{TR_C}} = -\lambda_{TR} R_{TR} \Omega_{TR} + w_{TR_C}$$

$$v_{i_{TR}} = -v_{i_{TR_C}} \cos K$$

The forces on the tail rotor in the cant axis system can be calculated using a transformation from cant-wind axes to cant axes:

$$X_{TR_C} = -H_{TR_{CW}} \cos \beta_{TR_C} - Y_{TR_{CW}} \sin \beta_{TR_C}$$

$$Y_{TR_C} = Y_{TR_{CW}} \cos \beta_{TR_C} - H_{TR_{CW}} \sin \beta_{TR_C}$$

$$Z_{TR_C} = -T_{TR_{CW}}$$

Similarly, through another transformation, the body axis forces and moments can be calculated:

$$X_{TR} = X_{TR_C}$$

$$Y_{TR} = -Z_{TR_C} \cos K + Y_{TR_C} \sin K$$

$$Z_{TR} = Y_{TR_C} \cos K + Z_{TR_C} \sin K$$

$$M_{TR} = -Q_{TR_{CW}} \cos K + Z_{TR}(STA_{TR} - STA_{c.g.}) - X_{TR}(WL_{TR} - WL_{c.g.})$$

$$L_{TR} = Y_{TR}(WL_{TR} - WL_{c.g.})$$

$$N_{TR} = Q_{TR_{CW}} \sin K - Y_{TR}(STA_{TR} - STA_{c.g.})$$

HORIZONTAL STABILATOR

The purpose of a horizontal stabilator with variable incidence is to eliminate excessively nose-high attitudes at low airspeed caused by downwash impingement on the stabilator and to optimize pitch attitudes for climb, cruise, and autorotational descent.

The position of the horizontal stabilator for the UH-60 is programmed between 8.0° trailing-edge-up and 39.0° trailing-edge-down as a function of four variables:

1. Airspeed
2. Collective Control Position
3. Pitch Rate
4. Lateral Acceleration

A detailed description of each of these four feedback loops is given in reference 2.

Figure 10 is a block diagram of the UH-60 horizontal stabilator control system (ref. 2). This logic has been incorporated in the generalized stability and control augmentation system of the math model. The stabilator logic also includes the provision for a fixed horizontal tail incidence that is to be specified by the pilot.

PITCH BIAS ACTUATOR

The UH-60's control system includes a pitch bias actuator (PBA), a variable length control rod which changes the relationship between longitudinal cyclic control and swashplate tilt as a function of three flight parameters: pitch attitude, pitch rate, and airspeed. The main purpose of the PBA is to improve the apparent static longitudinal stability of the aircraft. A detailed description of the PBA is given in reference 2.

The PBA was modeled directly from the block diagram shown in figure 11 (ref. 2). The airspeed feedback is only active between 80 and 180 knots since below 80 knots, the airspeed feedback for the stabilator performs the same stability function. The pitch attitude and rate feedback is active throughout the entire speed range. As can be seen from the block diagram, the PBA actuator authority is 15% of longitudinal cyclic full throw and has a maximum rate limit on the actuator travel of 3% per sec. The output of the PBA is added to the total longitudinal cyclic control. The PBA logic includes an on/off switch to inactivate the PBA, if desired.

UH-60 DESCRIPTION REQUIREMENTS

Table 1 lists the parameters required to model the UH-60 and the values used in the math model. This table is identical to table J-1 in reference 1, except that most of the required fuselage parameters have been eliminated because of the modifications to the fuselage aerodynamic model. The values listed for the UH-60 in table 1 were obtained from reference 2.

Table 2 lists the nonzero feedforward, crossfeed, and feedback gains for the UH-60 control system (see fig. 4 of ref. 1). A detailed description of the four control couplings is given in reference 2.

Table 3 lists the parameters that are required to model the two General Electric T700-GE-700 engines that power the UH-60 and the values that are used in the math model. These values are based on available T700-GE-700 engine data for the AH-64 helicopter.

UH-60 TRIM CHARACTERISTICS

Table 4 lists the four control positions, δ_e, δ_a, δ_c, and δ_p, the lateral and vertical velocities in body axes, v_B and w_B, and the Euler pitch and roll angles, θ and ϕ, for the UH-60 trimmed in level flight at a variety of airspeeds.

UH-60 STABILITY DERIVATIVES

Dimensional stability derivatives for the UH-60 math model are presented in tables 5 through 10. These derivatives were generated under the following conditions:

- level flight
- pitch bias actuator on
- horizontal stabilator active
- engine/governor model off

and with the following perturbation sizes:

$\Delta u_B = 1.0$ ft/sec

$\Delta v_B = 1.0$ ft/sec

$\Delta w_B = 1.0$ ft/sec

$\Delta p_B = 5.0$ deg/sec

$\Delta q_B = 5.0$ deg/sec

$\Delta r_B = 5.0$ deg/sec

$\Delta \delta_e = 0.1$ in.

$\Delta \delta_a = 0.1$ in.

$\Delta \delta_c = 0.1$ in.

$\Delta \delta_p = 0.1$ in.

The force and moment dimensional stability derivatives were obtained by considering both positive and negative perturbations about a reference trim condition. The derivatives are defined as follows:

$$X_{(\ )} = \frac{1}{m}\frac{\partial X}{\partial (\ )} \qquad M_{(\ )} = \frac{1}{I_{yy}}\frac{\partial M}{\partial (\ )}$$

$$Y_{(\ )} = \frac{1}{m}\frac{\partial Y}{\partial (\ )} \qquad L_{(\ )} = \frac{1}{I_{xx}}\frac{\partial L}{\partial (\ )}$$

$$Z_{(\ )} = \frac{1}{m}\frac{\partial Z}{\partial (\ )} \qquad N_{(\ )} = \frac{1}{I_{zz}}\frac{\partial N}{\partial (\ )}$$

MODEL VALIDATION

Validation of the UH-60 math model was accomplished by comparison of trim and stability derivative data that were generated from the UH-60 math model with data that were generated from a similar total force and moment math model of the UH-60, developed by Boeing-Vertol for the Advanced Digital/Optical Control System (ADOCS) program (ref. 4).

Tables 11 through 15 show level flight trim characteristics and dimensional stability derivatives generated by the Boeing-Vertol UH-60 math model for comparison with the data presented in tables 4 through 10. These derivatives were generated under the same conditions as the UH-60 derivatives were, but with significantly larger perturbation sizes, a slightly higher aircraft gross weight, and a faster main rotor rotational velocity. Figures 12 through 17 illustrate six of the more important UH-60 stability derivatives vs airspeed. For these plots, the UH-60 data are shown as well as the data generated from the Boeing-Vertol UH-60 math model.

CONCLUDING REMARKS

The mathematical model of a UH-60 helicopter described in this report was developed for real-time piloted simulation. To date, this model has been used successfully in two handling qualities simulation experiments on the six-degree-of-freedom Vertical Motion Simulator (VMS) at NASA Ames Research Center (refs. 5 and 6) in support of the ADOCS program.

For these simulations, however, high levels of stability augmentation were added to the baseline UH-60 math model, thus effectively masking many of the characteristics of the basic aircraft. The baseline UH-60 model has not been evaluated in real-time piloted simulations nor has it been validated with flight data to determine the accuracy with which it models the actual aircraft dynamics and handling qualities. In addition, neither the analog and digital stability augmentation system (SAS) nor the flight path stabilization (FPS) system of the actual UH-60 helicopter is included in the model.

REFERENCES

1. Talbot, P. D.; Tinling, B. E.; Decker, W. A.; and Chen, R. T. N.: A Mathematical Model of a Single Main Rotor Helicopter for Piloted Simulation. NASA TM-84281, September 1982.

2. Howlett, J. J.: UH-60A Black Hawk Engineering Simulation Program, Volumes I and II. NASA CR-166309 and CR-166310, December 1981.

3. Systems Control, Inc.: SCI Model Structure Determination Program (OSR) User's Guide. NASA CR-159084, November 1979.

4. Landis, K. H.; and Aiken, E. W.: An Assessment of Various Side-Stick Controller/ Stability and Control Augmentation Systems for Night Nap-of-the-Earth Flight Using Piloted Simulation. Helicopter Handling Qualities. NASA CP-2219, April 1982.

5. Landis, K. H.; Dunford, P. J.; Aiken, E. W.; and Hilbert, K. B.: A Piloted Simulator Investigation of Side-Stick Controller/Stability and Control Augmentation System Requirements for Helicopter Visual Flight Tasks. AHS Paper A-83-39-59-4000, May 1983.

6. Landis, K. H.; Glusman, S. I.; Aiken, E. W.; and Hilbert, K. B.: An Investigation of Side-Stick Controller/Stability and Control Augmentation System Requirements for Helicopter Terrain Flight Under Reduced Visibility Conditions. AIAA Paper 84-0235, January 1984.

TABLE 1.- UH-60 DESCRIPTION REQUIREMENTS

Description	Algebraic symbol	Computer mnemonic	Units	UH-60
Main rotor (MR) group				
MR rotor radius	R_{MR}	ROTOR	ft	26.83
MR chord	c_{MR}	CHORD	ft	1.73
MR rotational speed	Ω_{MR}	OMEGA	rad/sec	27.0
Number of blades	n_b	BLADES	N-D	4.0
MR Lock number	γ_{MR}	GAMMA	N-D	8.1936
MR hinge offset	ε	EPSLN	percent/100	.04659
MR flapping spring constant	K_β	AKBETA	lb-ft/rad	0
MR pitch-flap coupling tangent of δ_3	K_1	AKONE	N-D	0
MR blade twist	$\theta_{t_{MR}}$	THETT	rad	-.3142
MR precone angle (required for teetering rotor)	$a_{0_{MR}}$	AOP	rad	0
MR solidity	σ_{MR}	SIGMA	N-D	.08210
MR lift curve slope	a_{MR}	ASLOPE	rad^{-1}	5.73
MR maximum thrust	$C_{T_{max}}$	CTM	N-D	.1846
MR longitudinal shaft tilt (positive forward)	i_s	CIS	rad	.05236
MR hub stationline	STA_H	STAH	in.	341.2
MR hub waterline	WL_H	WLH	in.	315.0
Tail rotor (TR) group				
TR radius	R_{TR}	RTR	ft	5.5
TR rotational speed	Ω_{TR}	OMTR	rad/sec	124.62
TR Lock number	γ_{TR}	GAMATR	N-D	3.3783
TR solidity	σ_{TR}	STR	N-D	.1875
TR pitch-flap coupling tangent of δ_3	$K_{1_{TR}}$	FKITR	N-D	.7002
TR precone	$a_{0_{TR}}$	AOTR	rad	.01309
TR blade twist	$\theta_{t_{TR}}$	THETR	rad	-.3142
TR lift curve slope	a_{TR}	ATR	rad^{-1}	5.73
TR hub stationline	STA_{TR}	STATR	in.	732.0
TR hub waterline	WL_{TR}	WLTR	in.	324.7

TABLE 1.- CONTINUED

Description	Algebraic symbol	Computer mnemonic	Units	UH-60
Aircraft mass and inertia				
Aircraft weight	W_{ic}	WAITIC	lb	16400.0
Aircraft roll inertia	I_{XX}	XIXXIC	slug-ft^2	5629.0
Aircraft pitch inertia	I_{YY}	XIYYIC	slug-ft^2	40000.0
Aircraft yaw inertia	I_{ZZ}	XIZZIC	slug-ft^2	37200.0
Aircraft cross product of inertia	I_{YZ}	XIXZIC	slug-ft^2	1670.0
Center of gravity stationline	$STA_{c.g.}$	STACG	in.	360.4
Center of gravity waterline	$WL_{c.g.}$	WLCG	in.	247.2
Center of gravity buttline	$BL_{c.g.}$	BLCG	in.	0
Fuselage (Fus)				
Fus aerodynamic reference point stationline	STA_{ACF}	STAACF	in.	345.5
Fus aerodynamic reference point waterline	WL_{ACF}	WLACF	in.	234.0
Horizontal stabilizer (HS)				
HS station	STA_{HS}	STAHS	in.	700.4
HS waterline	WL_{HS}	WLHS	in.	244.0
HS incidence angle	i_{HS}	AIHS	rad	variable
HS area	S_{HS}	SHS	ft^2	45.0
HS aspect ratio	AR_{HS}	ARHS	N-D	4.6
HS maximum lift curve slope	$C_{L_{max_{HS}}}$	CLMHS	N-D	1.03
HS dynamic pressure ratio	η_{HS}	XNH	N-D	.4
Main rotor induced velocity effect at HS	$K_{V_{MR}}$	XKVMR	N-D	1.8
Vertical fin (VF)				
VF stationline	STA_{VF}	STAVF	in.	695.0
VF waterline	WL_{VF}	WLVF	in.	273.0
VF incidence angle	i_{VF}	AIFF	rad	0
VF area	S_{VF}	SF	ft^2	32.3
VF aspect ratio	AR_{VF}	ARF	N-D	1.92
VF sweep angle	Λ_F	ALMF	rad	.7156
VF maximum lift curve slope	$C_{L_{max_{VF}}}$	CLMF	N-D	.89
VF dynamic pressure ratio	η_{VF}	VNF	N-D	.651
Tail rotor induced velocity effect at VF	$k_{V_{TR}}$	XKVTR	N-D	1.0

TABLE 1.- CONCLUDED

Description	Algebraic symbol	Computer mnemonic	Units	UH-60
Controls				
Swashplate lateral cyclic pitch for zero lateral cyclic stick	$C_{A_{1S}}$	CAIS	rad	0
Swashplate longitudinal cyclic pitch for zero longitudinal cyclic stick	$C_{B_{1S}}$	CBIS	rad	0
Longitudinal cyclic control sensitivity	CK_1	CK1	rad/in.	.04939
Lateral cyclic control sensitivity	CK_2	CK2	rad/in.	.02792
Main rotor root collective pitch for zero collective stick	C_5	C5	rad	.2286
Main rotor collective control sensitivity	C_6	C6	rad/in.	.02792
Tail rotor root collective pitch for zero pedal position	C_7	C7	rad	.1743
Pedal sensitivity	C_8	C8	rad/in.	-.07734

TABLE 2.- UH-60 CONTROL SYSTEM CHARACTERISTICS

Description	Algebraic symbol	Computer mnemonic	UH-60
Feedforward gains	in./in.		
Longitudinal stick to longitudinal cyclic	δ_e/δ_{e_p}	SK(1)	1.0
Lateral stick to lateral cyclic	δ_a/δ_{a_p}	SK(5)	1.0
Collective stick to collective control	δ_c/δ_{c_p}	SK(9)	1.0
Pedals to directional control	δ_p/δ_{p_p}	SK(10)	1.0
Crossfeed gains			
Collective stick to longitudinal cyclic	δ_e/δ_{c_p}	SK(4)	-.1640
Pedals to longitudinal cyclic	δ_e/δ_{p_p}	SKM(2)	-.5746
Collective stick to lateral cyclic	δ_a/δ_{c_p}	SK(8)	-.16
Collective stick to directional control	δ_p/δ_{c_p}	SK(11)	-.2889
Feedback gains	in./rad/sec		
Pitch rate to lateral cyclic	δ_a/q_B	SKV(3,2)	1.3
Roll rate to longitudinal cyclic	δ_e/p_B	SKV(6,1)	-.88

TABLE 3.- UH-60 ENGINE CHARACTERISTICS

Description	Algebraic symbol	Computer mnemonic	Units	UH-60 T700-GE-700
Engine/governor				
Engine gain	K_E	HPK	HP/LB_{fuel}	1.75
Engine time constant	τ_E	HPT	sec	1.25
Throttle time constant	τ_t	THTAU	sec	1.25
Throttle position		THROT	%	100.0
MR rpm lower limit	Ω_{LIM}	OMLIM	rad/sec	9.0
Gear ratio	Ω_{TR}/Ω_{MR}	TRGEAR	N-D	4.62
Proportional governor feedback gain	K_{g_1}	GKG1	LB_{fuel}/rad/sec	2000.0
Integral governor feedback gain	K_{g_2}	GKG2	LB_{fuel}/rad/sec	2500.0
Rate governor feedback gain	K_{g_3}	GKG3	LB_{fuel}/rad/sec	500.0

TABLE 4.- LEVEL FLIGHT TRIM CHARACTERISTICS

Engineering symbol	Equivalent airspeed, knots						Units
	1.0	20.0	40.0	60.0	100.0	140.0	
δ_e	0.1266	-0.3670	-0.2083	-0.4238	-1.063	-1.800	in.
δ_a	.2321	-.9956	-.7560	-.2322	.1812	.3964	in.
δ_c	5.719	5.361	4.580	4.194	4.425	5.718	in.
δ_p	-1.279	-1.066	-.5830	-.5802	-.2606	-.005715	in.
v_B	-.006069	-.08037	-.08960	9.989	7.996	8.813	ft/sec
w_B	.1485	3.430	5.108	6.133	7.264	-1.235	ft/sec
θ	5.052	5.834	4.340	3.489	2.469	-.2996	deg
ϕ	-2.340	-1.342	-1.005	0	0	0	deg

TABLE 5.- X-FORCE STABILITY DERIVATIVES

Engineering symbol	Equivalent airspeed, knots						Units
	1.0	20.0	40.0	60.0	100.0	140.0	
X_u	-0.02349	-0.01040	-0.01122	-0.01900	-0.03238	-0.04063	1/sec
X_v	-.03402	-.02237	-.009834	-.002259	-.0005939	-.002359	1/sec
X_w	.02542	.03743	.04295	.04814	.06427	.07982	1/sec
X_q	2.809	2.828	3.221	3.352	2.788	1.626	ft/rad/sec
X_p	-.2585	-.1883	-.05796	.01583	-.1132	-.3844	ft/rad/sec
X_r	-.2071	-.1151	-.01708	-.08981	-.06855	-.05904	ft/rad/sec
X_{δ_e}	-1.659	-1.582	-1.498	-1.402	-1.083	-.7098	ft/in./sec^2
X_{δ_a}	.04358	.03288	.01803	.01082	-.01658	-.009678	ft/in./sec^2
X_{δ_c}	.9709	.9707	.7004	.5931	.6461	.6144	ft/in./sec^2
X_{δ_p}	.9544	.9143	.8656	.8695	.6988	.5020	ft/in./sec^2

TABLE 6.- Z-FORCE STABILITY DERIVATIVES

Engineering symbol	Equivalent airspeed, knots						Units
	1.0	20.0	40.0	60.0	100.0	140.0	
Z_u	0.02274	-0.1460	-0.1252	-0.04741	-0.008851	0.0003375	1/sec
Z_v	-.008874	-.02547	-.01531	-.02032	-.01720	-.04257	1/sec
Z_w	-.2931	-.3834	-.5617	-.6696	-.7897	-.8696	1/sec
Z_q	.3604	2.237	2.865	3.502	4.981	6.638	ft/rad/sec
Z_p	-.01037	.3402	.8662	1.358	2.676	3.935	ft/rad/sec
Z_r	-.2059	-.3000	-.4176	-.4981	-.5056	-.3598	ft/rad/sec
Z_{δ_e}	-.1372	-1.037	-2.030	-3.271	-6.138	-9.118	ft/in./sec^2
Z_{δ_a}	.004142	.04533	.09963	.3733	.5627	.8477	ft/in./sec^2
Z_{δ_c}	-7.921	-7.377	-7.478	-8.324	-9.630	-10.76	ft/in./sec^2
Z_{δ_p}	.5791	1.074	1.626	2.372	3.995	5.543	ft/in./sec^2

TABLE 7.- Y-FORCE STABILITY DERIVATIVES

Engineering symbol	Equivalent airspeed, knots						Units
	1.0	20.0	40.0	60.0	100.0	140.0	
Y_u	0.03381	0.01808	0.002607	-0.003401	-0.0007094	0.001946	1/sec
Y_v	-.04733	-.05825	-.08184	-.1044	-.1430	-.1838	1/sec
Y_w	.004331	.006895	.008117	.01029	.01025	.007387	1/sec
Y_q	-.3585	-.002115	.2133	.4611	.7513	.9988	ft/rad/sec
Y_p	-1.723	-1.972	-2.381	-2.608	-2.610	-2.228	ft/rad/sec
Y_r	.6383	.5788	.9683	1.249	1.658	2.051	ft/rad/sec
Y_{δ_e}	.07659	.04994	.03957	.02118	-.01624	-.07161	ft/in./sec^2
Y_{δ_a}	.9420	.9542	.9389	.9284	.9305	.9674	ft/in./sec^2
Y_{δ_c}	.1005	.06201	.1970	.2470	.3408	.3814	ft/in./sec^2
Y_{δ_p}	-1.486	-1.338	-1.359	-1.587	-1.941	-2.176	ft/in./sec^2

TABLE 8.- M-MOMENT STABILITY DERIVATIVES

Engineering symbol	Equivalent airspeed, knots						Units
	1.0	20.0	40.0	60.0	100.0	140.0	
M_u	0.003554	0.001085	-0.0002337	0.001929	0.002507	0.005558	rad/ft/sec
M_v	.01350	.01115	.007824	.006016	.001636	-.007029	rad/ft/sec
M_w	.002024	.003433	.006749	.008916	.009212	.008923	rad/ft/sec
M_q	-.8161	-.8910	-1.067	-1.230	-1.606	-2.015	1/sec
M_p	.3139	.2894	.2468	.2008	.1031	.007006	1/sec
M_r	-.003352	-.02974	-.08964	-.1130	-.1039	-.02461	1/sec
M_{δ_e}	.3346	.3516	.3721	.3997	.4594	.5230	rad/in./sec^2
M_{δ_a}	-.003559	-.003824	-.001497	.005281	.02829	.06496	rad/in./sec^2
M_{δ_c}	-.005557	.02730	.06350	.08925	.09507	.1029	rad/in./sec^2
M_{δ_p}	.01538	-.006399	-.02969	-.03336	-.07520	-.1707	rad/in./sec^2

TABLE 9.- L-MOMENT STABILITY DERIVATIVES

Engineering symbol	Equivalent airspeed, knots						Units
	1.0	20.0	40.0	60.0	100.0	140.0	
L_u	0.07627	0.02327	-0.007782	-0.006377	-0.002139	0.001610	rad/ft/sec
L_v	-.04124	-.03956	-.03447	-.03690	-.03737	-.03928	rad/ft/sec
L_w	.005022	.01749	.02836	.02586	.02264	.01740	rad/ft/sec
L_q	-2.272	-1.730	-1.566	-1.522	-1.424	-1.269	1/sec
L_p	-3.551	-3.604	-3.819	-3.954	-3.911	-3.626	1/sec
L_r	.07467	.04429	.2726	.4375	.6039	.7766	1/sec
L_{δ_e}	.04363	.04924	.1010	.1210	.1502	.1426	rad/in./sec^2
L_{δ_a}	1.334	1.339	1.329	1.316	1.316	1.332	rad/in./sec^2
L_{δ_c}	-.1471	-.03080	.1981	.2095	.2580	.2719	rad/in./sec^2
L_{δ_p}	-.8406	-.7759	-.7967	-.9414	-1.163	-1.300	rad/in./sec^2

TABLE 10.- N-MOMENT STABILITY DERIVATIVES

Engineering symbol	Equivalent airspeed, knots						Units
	1.0	20.0	40.0	60.0	100.0	140.0	
N_u	0.002149	-0.005618	-0.005796	-0.003739	-0.002896	-0.003813	rad/ft/sec
N_v	.009759	.008566	.01245	.01529	.01823	.01979	rad/ft/sec
N_w	-.001943	-.003705	-.006419	-.01079	-.01253	-.007266	rad/ft/sec
N_q	-.3396	-.7563	-.5837	-.4874	-.4424	-.5254	1/sec
N_p	-.1013	-.2857	-.2310	-.1499	-.1136	-.1801	1/sec
N_r	-.3342	-.3662	-.5336	-.6547	-.8515	-1.011	1/sec
N_{δ_e}	.001120	-.009063	-.01760	-.03105	-.04719	.005004	rad/in./sec^2
N_{δ_a}	.02734	.02695	.02598	.02691	.02582	.02299	rad/in./sec^2
N_{δ_c}	.06306	.06005	.01613	-.04757	-.1096	-.08942	rad/in./sec^2
N_{δ_p}	.6040	.5550	.5701	.6785	.8460	.9274	rad/in./sec^2

TABLE 11. - LEVEL FLIGHT TRIM CHARACTERISTICS
BOEING-VERTOL UH-60 MATH MODEL

Engineering symbol	Equivalent airspeed, knots						Units
	0.5	20.0	40.0	60.0	100.0	140.0	
δ_e	1.1947	0.5938	0.3636	0.5149	-0.5356	-1.0539	in.
δ_a	.4393	-.7920	-.7106	-.3199	-.1098	-.0917	in.
δ_c	5.3976	5.0054	4.2440	3.8582	4.2054	5.6883	in.
δ_p	-.2598	-.2409	-.05631	-.1254	.0974	.1798	in.
v_B	0	0	0	13.165	9.4517	11.308	ft/sec
w_B	0	4.0507	6.5824	3.8820	4.8946	-13.840	ft/sec
θ	5.1186	6.9262	5.5167	2.2425	1.6799	-3.3533	deg
ϕ	-2.5666	-1.6093	-1.2929	0	0	0	deg

TABLE 12.- X, Y, AND Z-FORCE STABILITY DERIVATIVES
BOEING-VERTOL UH-60 MATH MODEL

Engineering symbol	Equivalent airspeed, knots						Units
	0.5	20.0	40.0	60.0	100.0	140.0	
X_u	-0.0150	0.0184	-0.0274	-0.0201	-0.0422	-0.0517	1/sec
X_{δ_e}	-1.7041	-1.5711	-1.3039	-1.2532	-.7256	-.2927	ft/in./sec^2
Y_v	-.0465	-.0523	-.0693	-.0950	-.1336	-.1749	1/sec
Y_{δ_a}	.9664	.9648	.9417	.9148	.9364	.9924	ft/in./sec^2
Y_{δ_p}	-1.7151	-1.6223	-1.6140	-1.7968	-2.1322	-2.3677	ft/in./sec^2
Z_u	-.0050	-.1573	-.1332	-.0546	-.0158	-.0324	1/sec
Z_w	-.2748	-.3475	-.5395	-.6523	-.7658	-.8418	1/sec
Z_{δ_e}	-.1134	-1.0026	-1.8678	-3.0911	-5.8800	-8.8178	ft/in./sec^2
Z_{δ_c}	-8.5829	-8.1266	-7.8250	-9.0061	-10.4761	-11.8225	ft/in./sec^2
Z_{δ_p}	.6799	1.1830	1.7228	2.5612	4.3935	6.3606	ft/in./sec^2

TABLE 13.- M-MOMENT STABILITY DERIVATIVES
BOEING-VERTOL UH-60 MATH MODEL

Engineering symbol	Equivalent airspeed, knots						Units
	0.5	20.0	40.0	60.0	100.0	140.0	
M_u	0.0005	0.0091	-0.0043	0.0040	0.0022	0.0019	rad/ft/sec
M_v	.0085	.0022	-.0006	.0011	-.0019	-.0068	rad/ft/sec
M_w	.0021	.0122	.0050	.0072	.0082	.0113	rad/ft/sec
M_q	-.7674	-1.0262	-1.2832	-1.5541	-1.9808	-2.1616	1/sec
M_p	.2938	.2859	.2567	.2379	.1797	.1937	1/sec
M_r	-.0688	-.0595	-.1181	-.1149	-.0860	-.0750	1/sec
M_{δ_e}	.3287	.3366	.3850	.4133	.4543	.4997	rad/in./sec^2
M_{δ_a}	-.0051	.0042	.0134	.0128	.0397	.0585	rad/in./sec^2
M_{δ_c}	-.0183	-.0352	.1574	.1362	.1294	.1418	rad/in./sec^2
M_{δ_p}	.0411	-.0010	-.0499	-.0562	-.0881	-.1113	rad/in./sec^2

TABLE 14.- L-MOMENT STABILITY DERIVATIVES
BOEING-VERTOL UH-60 MATH MODEL

Engineering symbol	Equivalent airspeed, knots						Units
	0.5	20.0	40.0	60.0	100.0	140.0	
L_v	-0.0260	-0.0250	-0.0267	-0.0258	-0.0304	-0.0343	rad/ft/sec
L_q	-1.7256	-1.8067	-1.5485	-1.4919	-1.3987	-1.4051	1/sec
L_p	-3.3484	-3.5455	-3.7116	-3.7659	-3.6853	-3.3574	1/sec
L_r	.2119	.3507	.4149	.4878	.6814	.8556	1/sec
L_{δ_a}	1.3118	1.3297	1.3147	1.2866	1.2907	1.3128	rad/in./sec^2
L_{δ_p}	-.9313	-.8816	-.8968	-1.0035	-1.1990	-1.3063	rad/in./sec^2

TABLE 15.- N-MOMENT STABILITY DERIVATIVES
BOEING-VERTOL UH-60 MATH MODEL

Engineering symbol	Equivalent airspeed, knots						Units
	0.5	20.0	40.0	60.0	100.0	140.0	
N_v	0.0081	0.0108	0.0119	0.0141	0.0176	0.0195	rad/ft/sec
N_p	-.1856	.0322	.0251	-.0446	-.0706	-.0955	1/sec
N_r	-.2879	-.3902	-.5142	-.6283	-.8389	-1.0394	1/sec
N_{δ_a}	.0266	-.0286	-.0268	-.0110	.0014	.0032	rad/in./sec^2
N_{δ_c}	.0665	.0576	.0222	-.0191	-.0544	-.0041	rad/in./sec^2
N_{δ_p}	.7153	.6731	.6720	.7668	.9319	1.0023	rad/in./sec^2

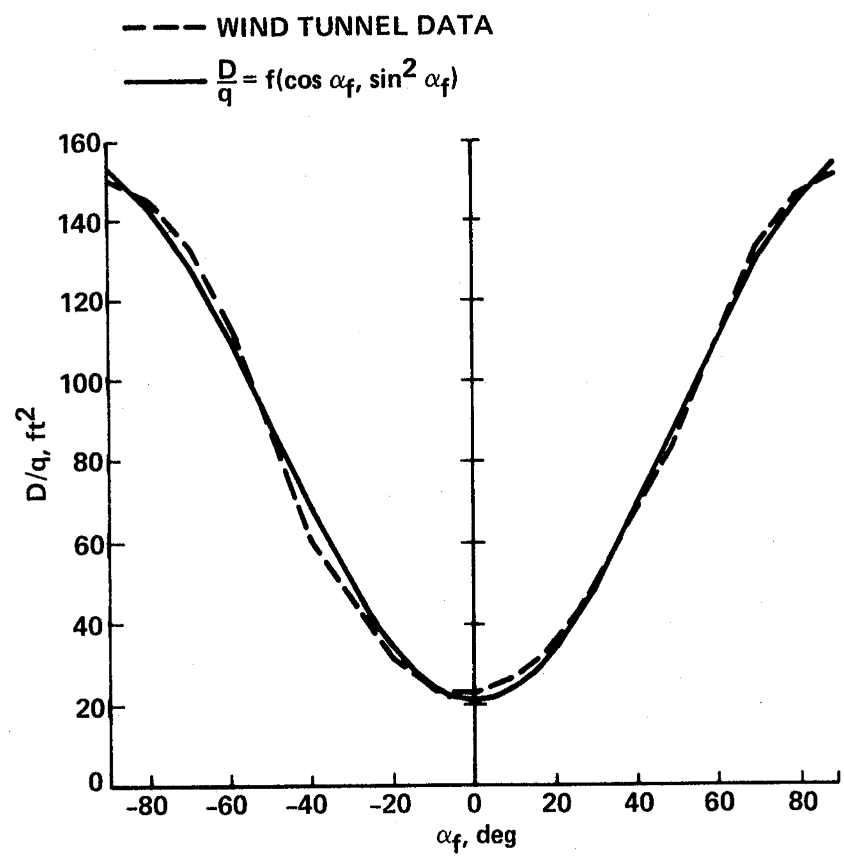

Figure 1.- Fuselage drag vs angle of attack.

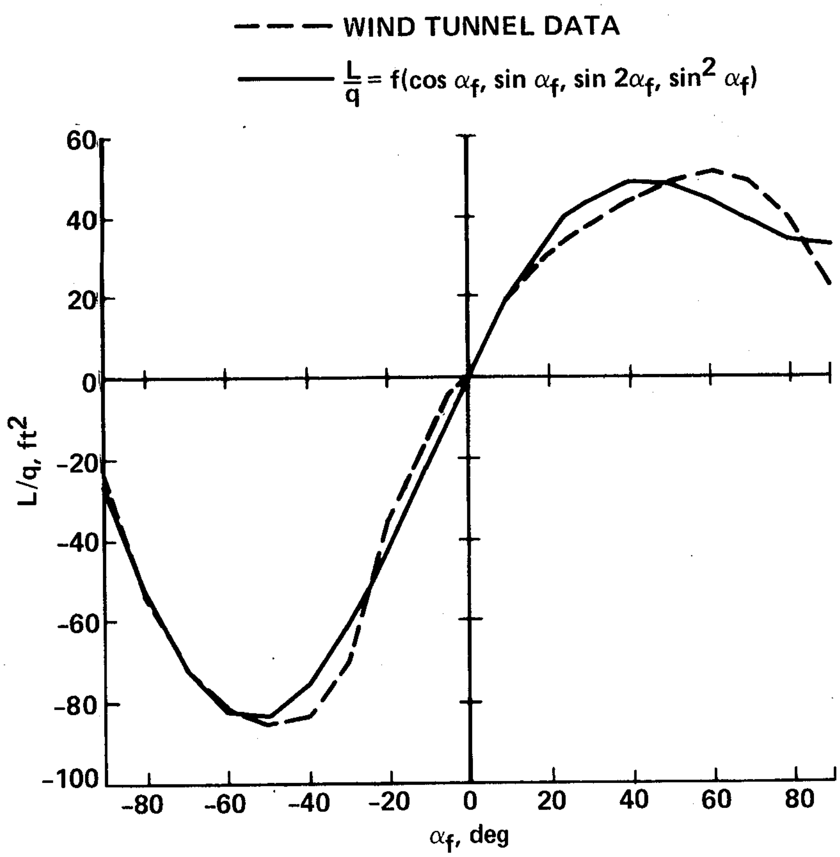

Figure 2.- Fuselage lift vs angle of attack.

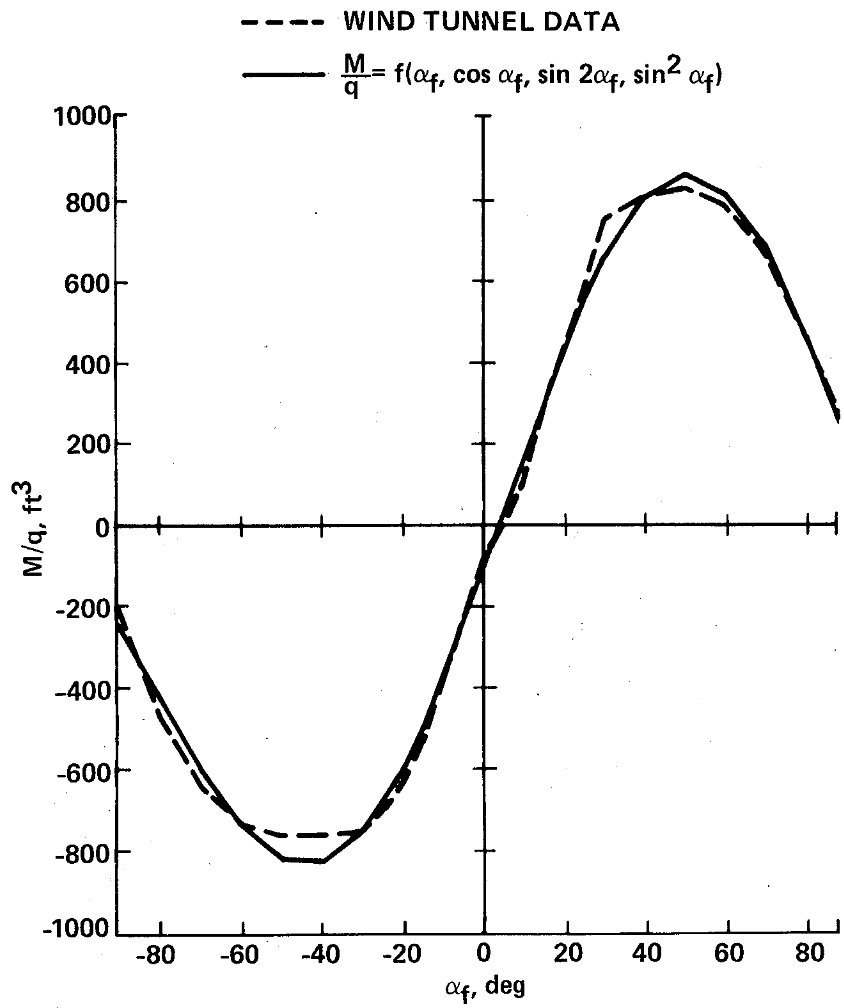

Figure 3.- Fuselage pitching moment vs angle of attack.

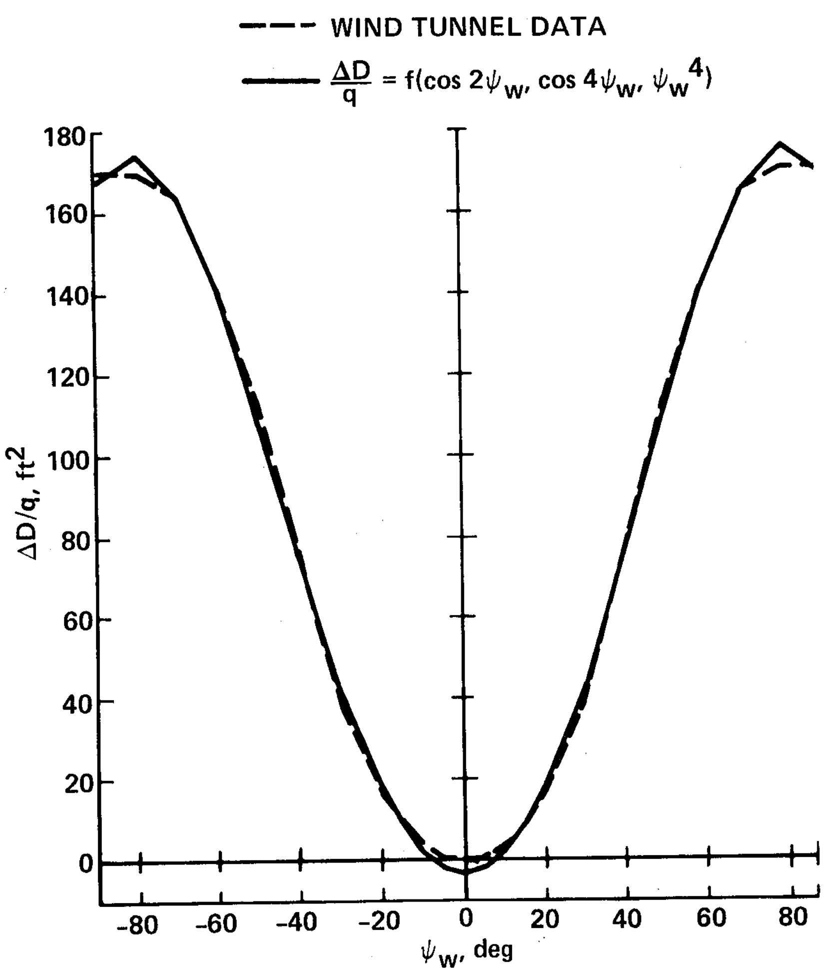

Figure 4.- Incremental fuselage drag vs sideslip.

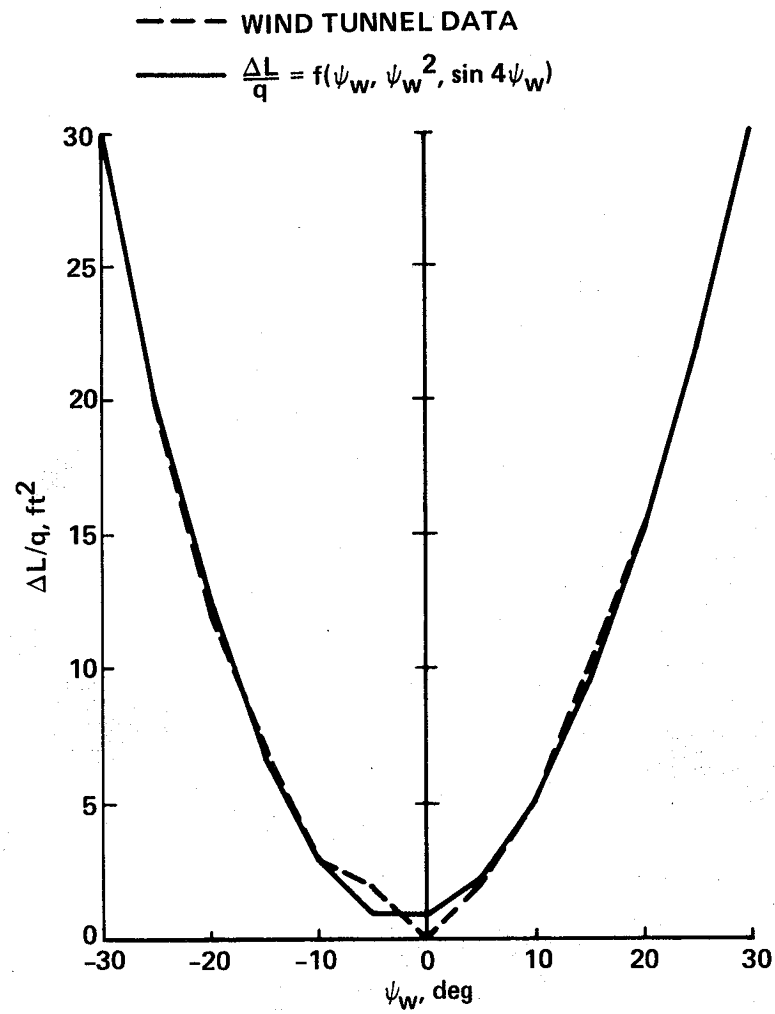

Figure 5.- Incremental fuselage lift vs sideslip.

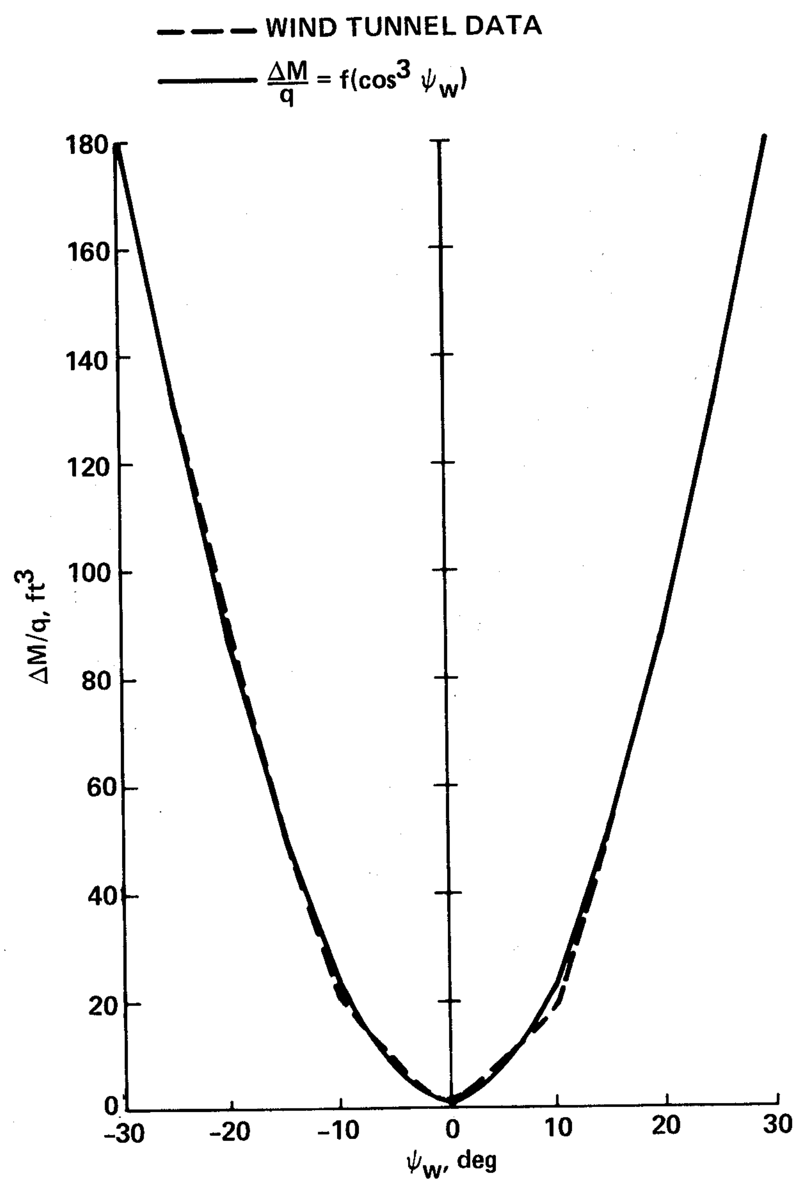

Figure 6.- Incremental fuselage pitching moment vs sideslip.

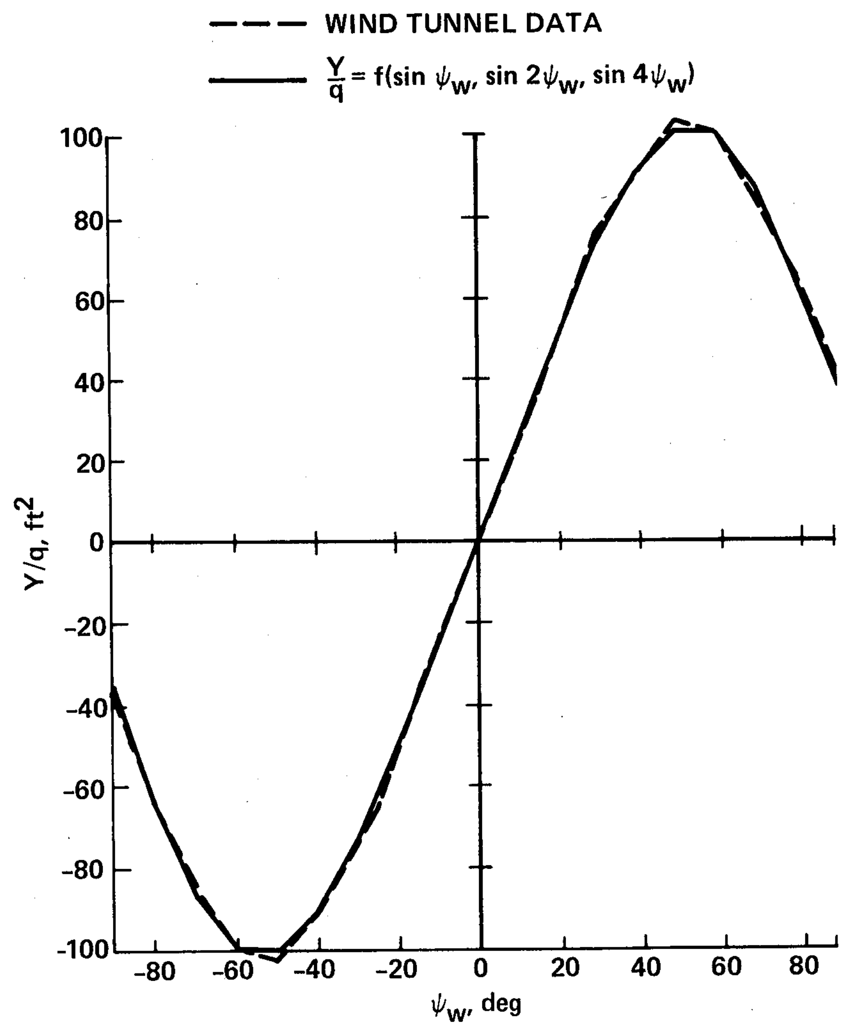

Figure 7.- Fuselage side force vs sideslip.

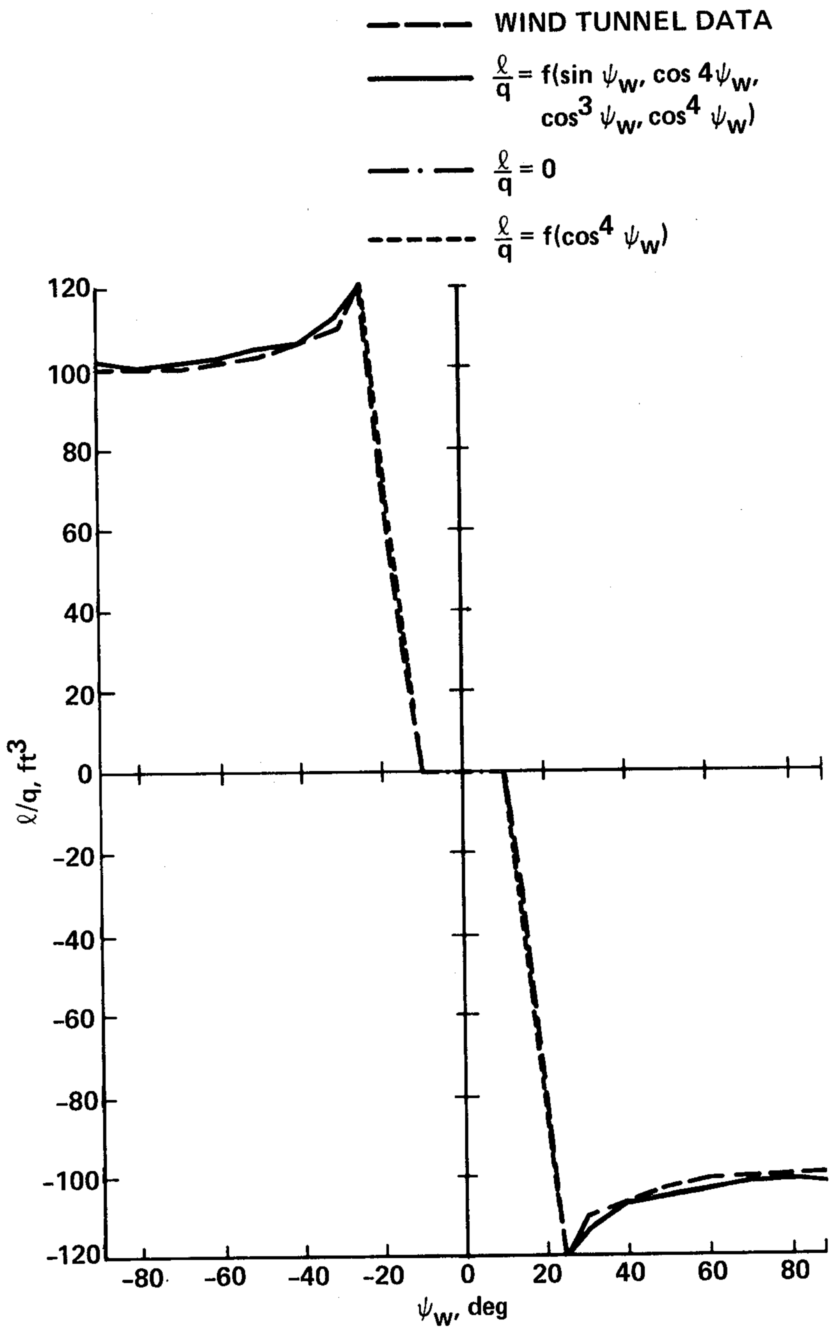

Figure 8.- Fuselage rolling moment vs sideslip.

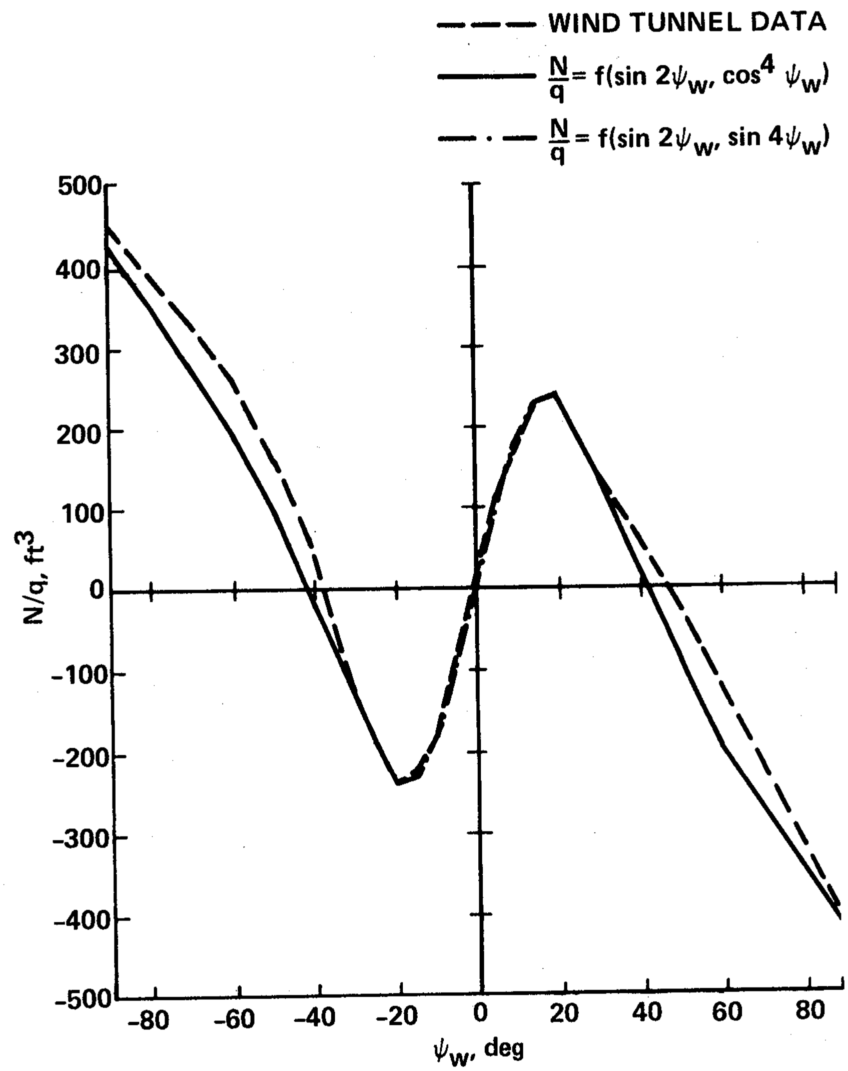

Figure 9.- Fuselage yawing moment vs sideslip.

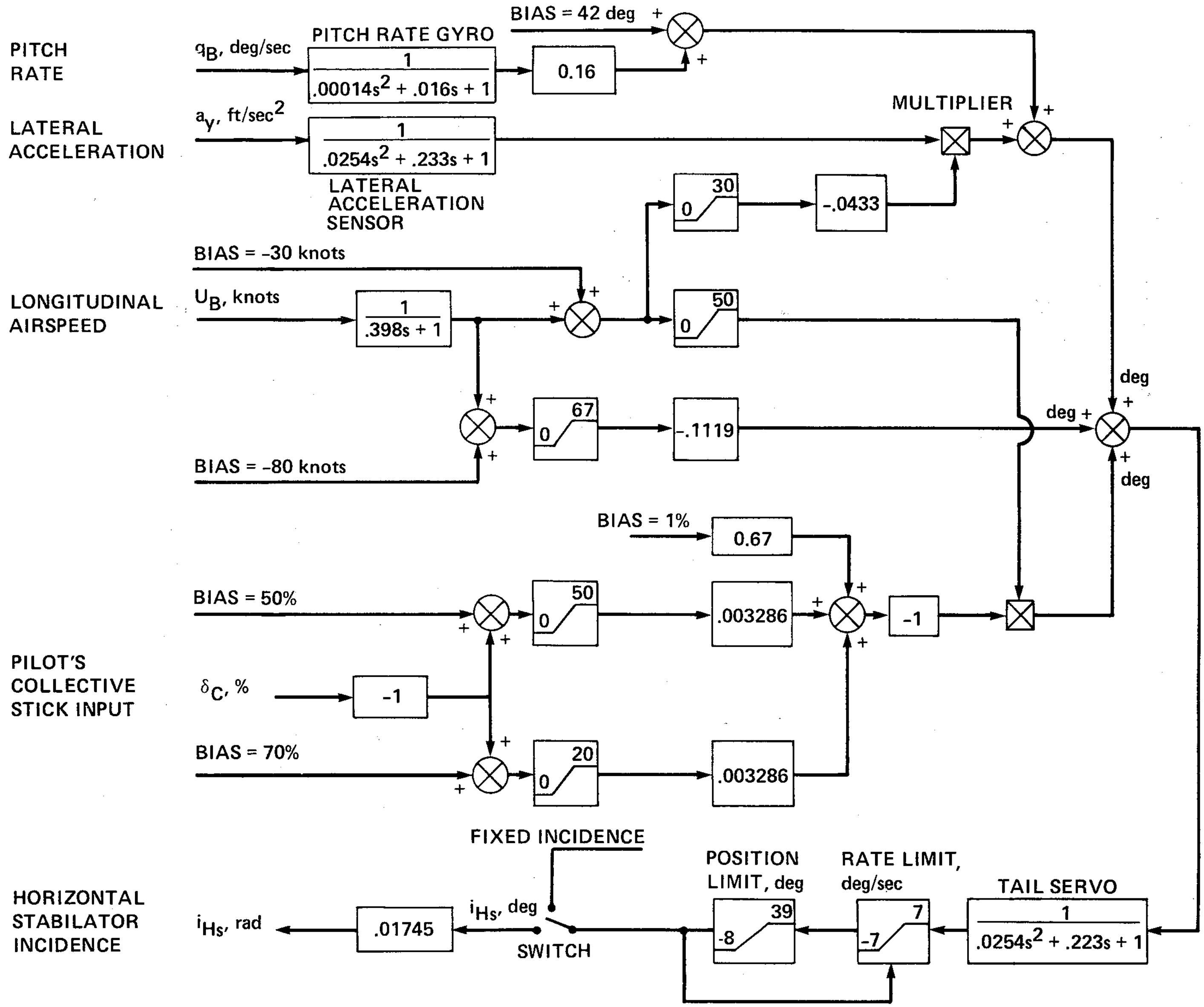

Figure 10.- UH-60 horizontal stabilator control system.

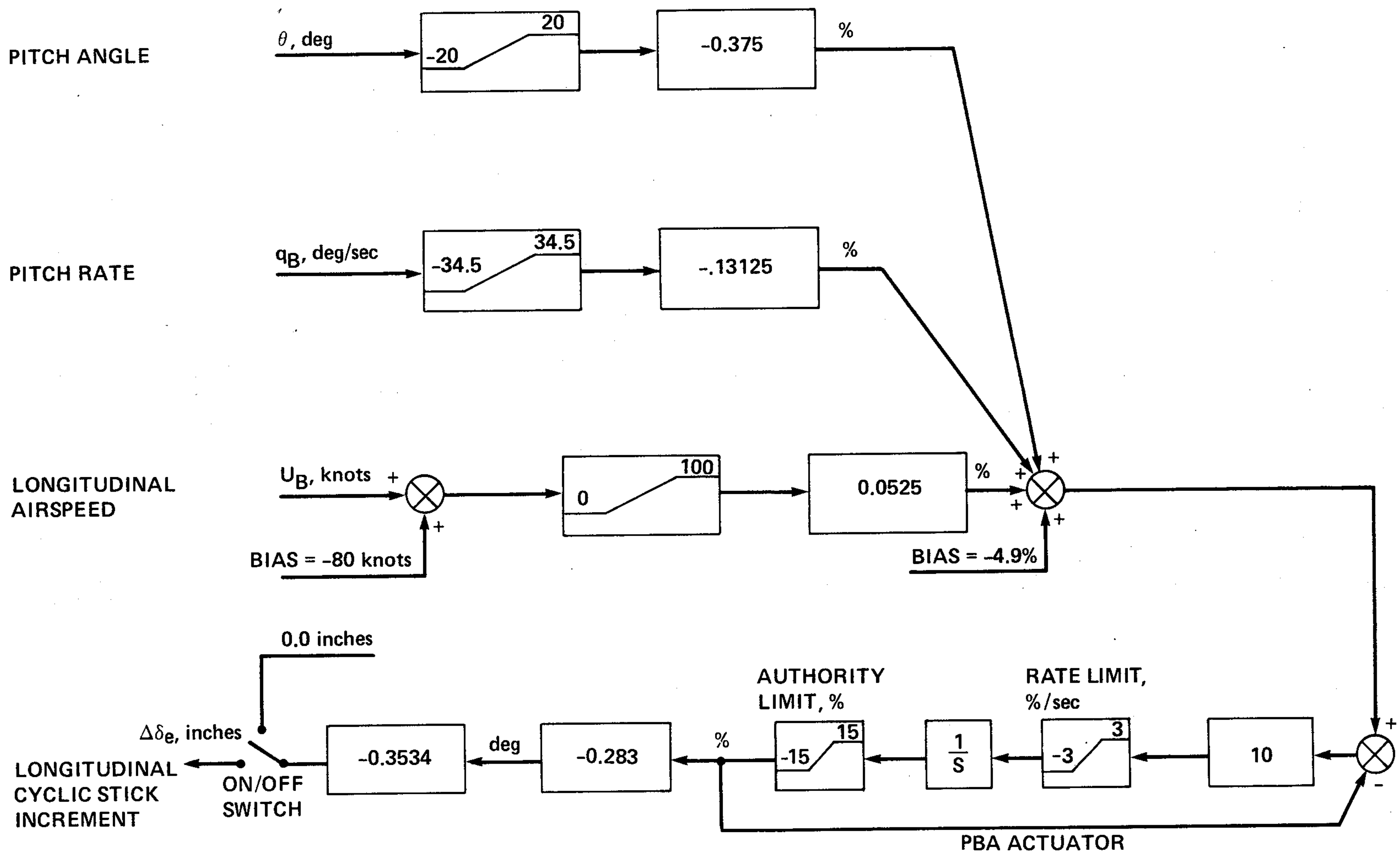

Figure 11.- UH-60 pitch bias actuator.

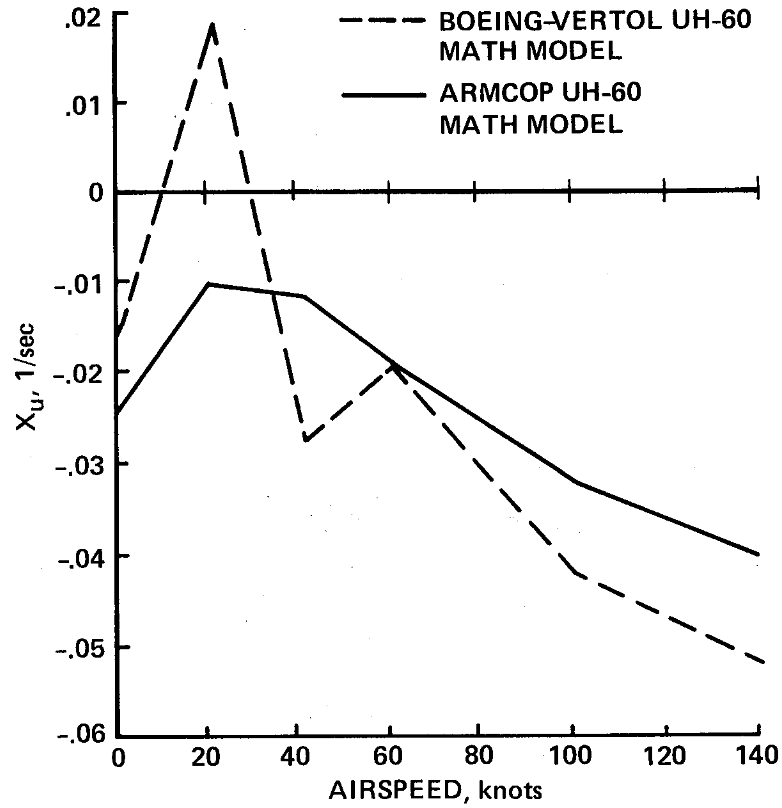

Figure 12.- Drag damping vs airspeed.

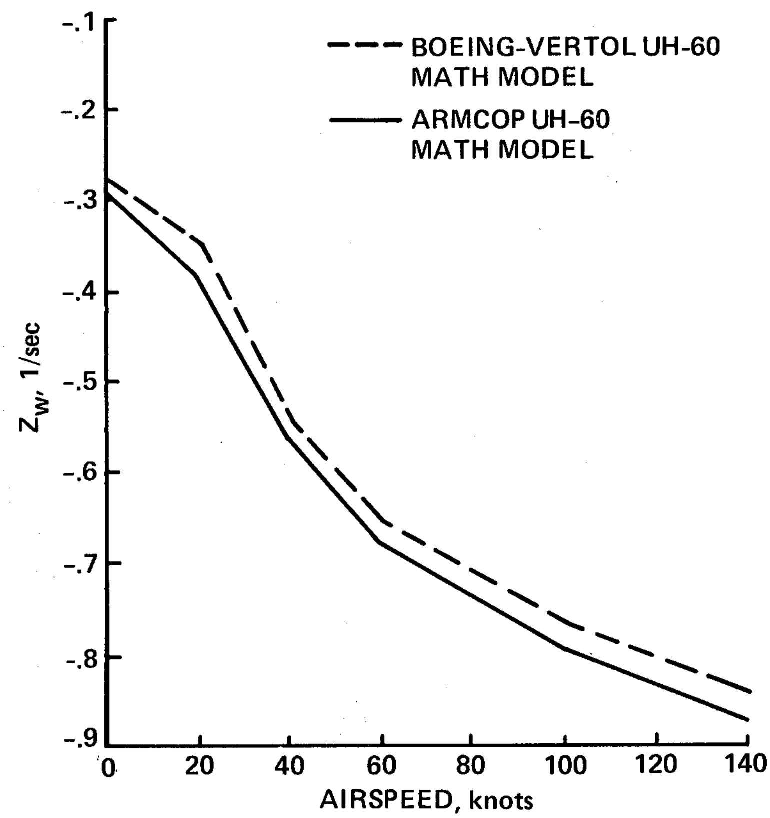

Figure 13.- Vertical damping vs airspeed.

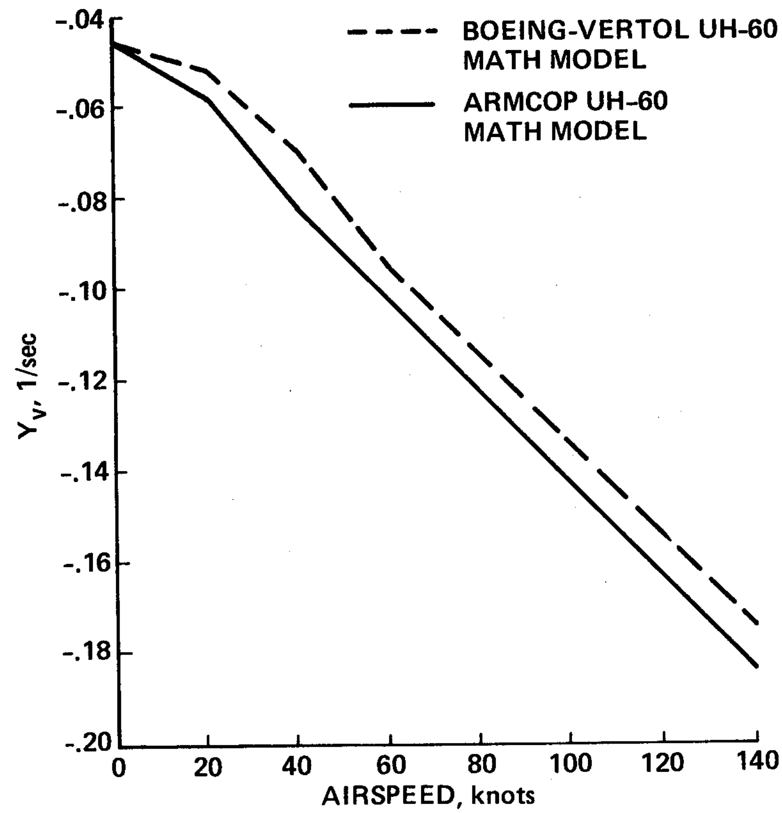

Figure 14.- Side-force damping vs airspeed.

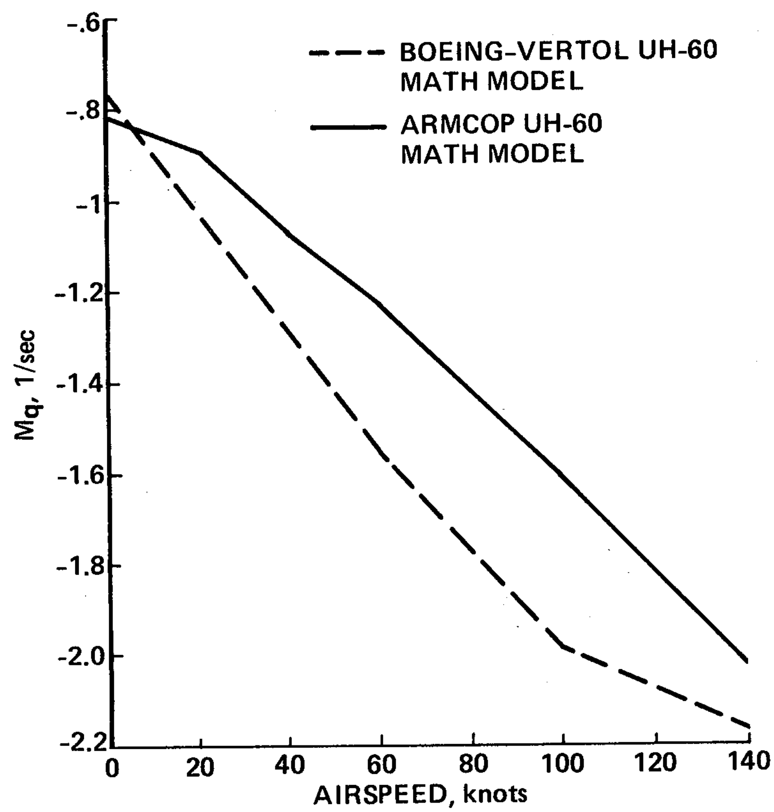

Figure 15.- Pitch damping vs airspeed.

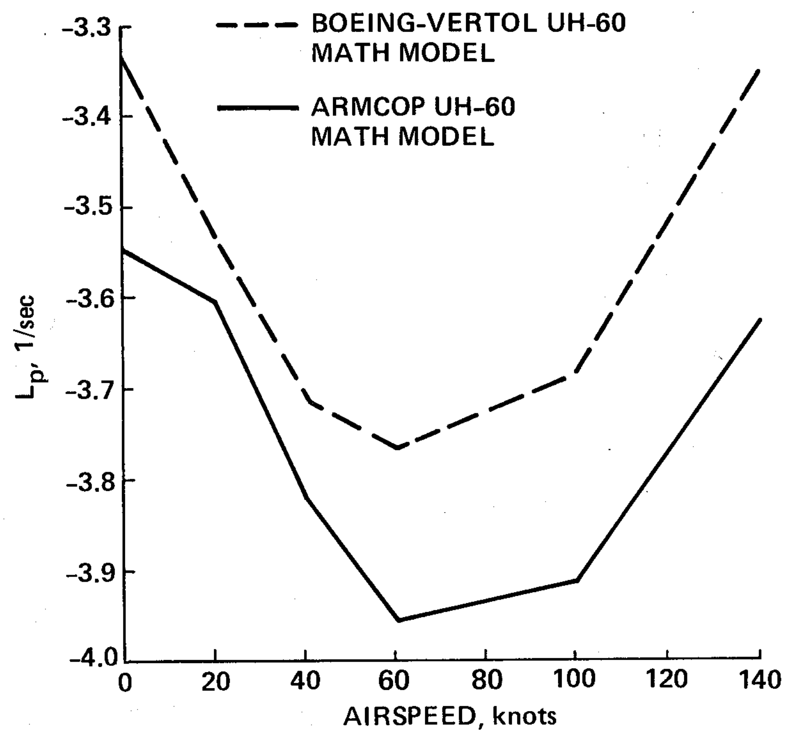

Figure 16.- Roll damping vs airspeed.

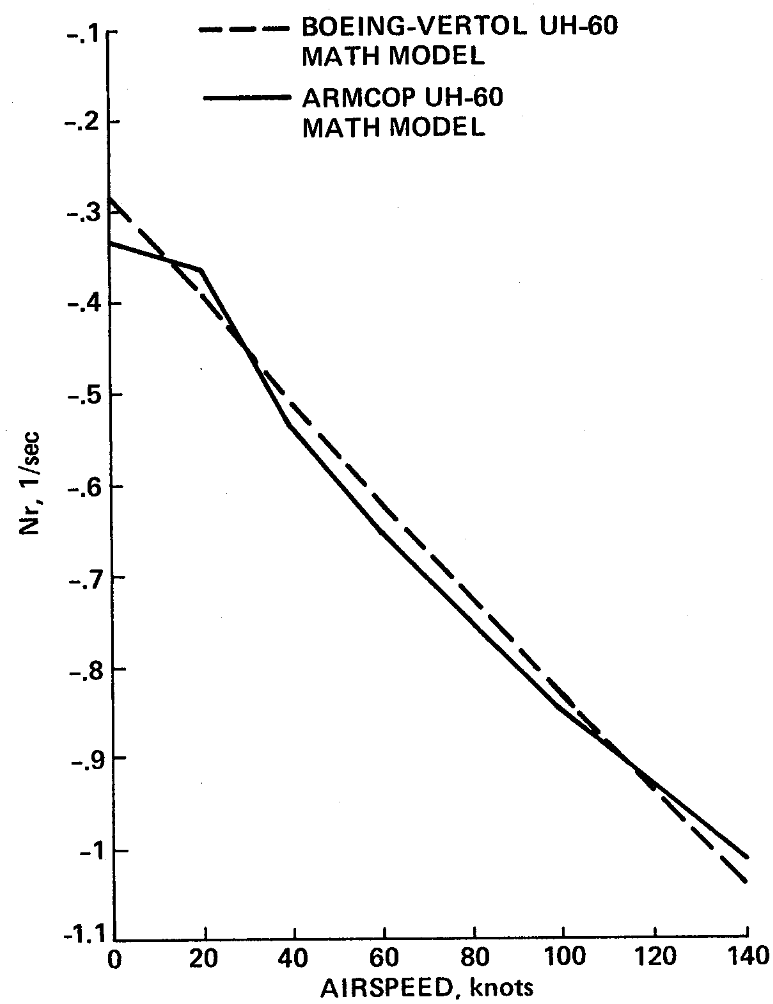

Figure 17.- Yaw damping vs airspeed.

1. Report No. NASA TM 85890 and USAAVSCOM TM-84-A-2

2. Government Accession No.

3. Recipient's Catalog No.

4. Title and Subtitle
A MATHEMATICAL MODEL OF THE UH-60 HELICOPTER

5. Report Date
April 1984

6. Performing Organization Code

7. Author(s)
Kathryn B. Hilbert

8. Performing Organization Report No.
A-9646

10. Work Unit No.
T-6292

9. Performing Organization Name and Address
Ames Research Center and Aeromechanics Laboratory, U. S. Army Research and Technology Laboratories -- AVSCOM, Ames Research Center, Moffett Field, CA. 94035

11. Contract or Grant No.

12. Sponsoring Agency Name and Address
National Aeronautics and Space Administration, Washington, D. C. 20546 and US Army Aviation Systems Command, St. Louis, MO. 63120

13. Type of Report and Period Covered
Technical Memorandum

14. Sponsoring Agency Code
505-42-11

15. Supplementary Notes
Point of Contact: Kathryn B. Hilbert, MS 211-2, Moffett Field, CA. 94035
(415) 965-5272 or FTS 448-5272

16. Abstract This report documents the revisions made to a ten-degree-of-freedom, full-flight envelope, generic helicopter mathematical model to represent the UH-60 helicopter accurately. The major modifications to the model include fuselage aerodynamic force and moment equations specific to the UH-60, a canted tail rotor, a horizontal stabilator with variable incidence, and a pitch bias actuator (PBA). In addition, this report presents a full set of parameters and numerical values which describe the helicopter configuration and physical characteristics.

Model validation was accomplished by comparison of trim and stability derivative data generated from the UH-60 math model with data generated from a similar total force and moment math model.

17. Key Words (Suggested by Author(s)) Helicopter, Helicopter Aerodynamics, UH-60, Canted tail rotor, Horizontal stabilizer, Pitch bias actuator, Stability derivatives, Mathematical model, Simulator

18. Distribution Statement
Unlimited

Subject category 08

19. Security Classif. (of this report)
Unclassified

20. Security Classif. (of this page)
Unclassified

21. No. of Pages
45

22. Price*
A03

*For sale by the National Technical Information Service, Springfield, Virginia 22161